Temperature and Energy Dependence of Proton Dechanneling in Silicon

G. Foti, F. Grasso, R. Quattrocchi, and E. Rimini
Centro Siciliano di Fisica Nucleare e di Struttura della Materia and Gruppo Nazionale di Struttura della Materia del Consiglio Nazionale delle Ricerche and Istituto di Struttura della Materia, Università di Catania, Catania, Italy 95129

(Received 25 May 1970; revised manuscript received 20 October 1970)

The dechanneled fractions of protons impinging along the ⟨111⟩ and ⟨110⟩ axial directions of Si have been measured for ion energies between 0.3 and 1.5 MeV and for target temperatures ranging between 80 and 423 °K. The dechanneled fraction is a linear function of the penetration depth z. Its dependence on beam energy E and the target temperature T can be described simply through the parameter $z\rho^2/E$, ρ^2 being the mean-square vibrational amplitude normal to the row. All the experimental points follow a unique linear trend if plotted vs $z\rho^2/E$. The dechanneled fraction for the ⟨110⟩ axis is a factor of 2 lower than that for the ⟨111⟩. A theoretical model has been developed to describe the dechanneling in terms of a steady increase in the transverse energy, accounting for both electronic and nuclear reduced multiple scattering. The initial transverse-energy distribution of the particle just beneath the crystal surface has been computed including the experimental angular spread, and both scatterings produced by the amorphous layers covering the surface and by the atomic string potential. The limiting transverse energy for the channeled-to-random transition has been taken from the experimental $\psi_{1/2}(T)$ values. The computed dechanneled fractions agree reasonably well with the experimental ones and justify their temperature and energy dependence. The calculated fractions differ from the experimental ones in their having an upward curvature; the significance of this disagreement is briefly discussed together with the approximations involved.

I. INTRODUCTION

Several experiments on channeling have been reported concerning mainly the determination of the critical angles, the energy losses, and ranges of energetic ions impinging on single crystals.[1,2]

The interpretation of these phenomena has been developed on the basis of a classical theory[1,3] which, except for some quantum-mechanical corrections,[4] justifies the experimental results. In this theory[1,3] the motion of a particle inside a channel is governed by a potential which is constant in the longitudinal direction and whose magnitude is obtained from an average of the atomic potentials. As a consequence, the transverse energy of the ion is conserved and the impinging beam can be divided into two parts, one aligned and one random. In the above scheme transitions between these two cannot occur.

The experimental results indeed show that transitions are possible, as evidenced by the dechanneling,[5,6] and therefore the transverse energy along the path is not conserved. This nonconservation is due to the scattering of the moving ion by nuclei and electrons of the crystal. A first theoretical basis for the interpretation of these phenomena has been proposed by Linkhard.[3]

Among the experimental results so far obtained about the dechanneling, the following ones may be quoted: Davies *et al.*[5] have measured in detail, by backscattering of protons and α particle the dechanneling in the ⟨110⟩ axis and {110} plane of W at temperatures between 25 and 450 °C. The authors found an exponential decrease in the channeled fraction with the penetration depth. To explain these results they introduce a mean free path for the channeled particles. About the same exponential trend has been observed by Andersen *et al.*[7] in the yield of a (p,γ) reaction in Al.

Ellegard *et al.*[8] have performed similar measurements in Bi at 80 and 300 °K; they explain the results assuming a linear increase in the mean-square angular width of the beam with the distance transversed.

Appleton *et al.*[6] have investigated the planar case by transmission measurements of protons in Si. The authors assume a diffusion process which produced a progressive spreading of the beam with the penetration.[9]

They propose a multiple electronic scattering mechanism as responsible for such a spreading. On the same basis the dechanneling of protons in Ge[10] and of high-energy protons in Si[11] has been treated.

The authors in a preliminary report[12] tried to find the functional temperature dependence of the dechanneled fraction. Our results suggested that nuclear scattering should be taken into account and encouraged the extension of the work to give a wider experimental support to the theoretical approach. The experimental determination of the dechanneling dependence on penetration depth, crys-

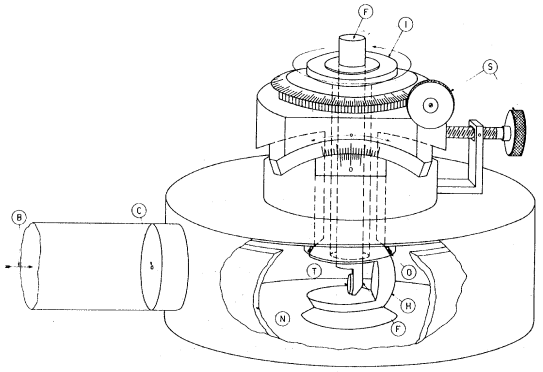

FIG. 1. Scattering chamber and goniometer assembly: T, single-crystal target; F, metallic-finger pipe; H, spherical holder; O, O-ring; I, thermal insulator; S, micrometer screws; H, beam entrance; C, circular aperture; and N, liquid-nitrogen trap.

tal temperature, and ion energy seems, in fact, to be one of the more powerful methods for a direct investigation of the changes in the transverse energy.

The present paper describes some measurements performed by the backscattering technique on the dechanneling rate as a function of penetration depth for protons of 0.3, 0.6, and 1.5 MeV along the ⟨111⟩ and ⟨110⟩ axes of Si at temperatures between 80 and 423 °K.

In connection with these experimental results a physical model for axial dechanneling has been developed following Lindhard's[3] point of view. The calculations have been carried out for protons impinging along the ⟨111⟩ axis of Si for a direct comparison with the experimental results. The experimental arrangement and the results obtained are reported in Secs. II and III, while the theoretical model and the calculations are discussed in Secs. IV and V.

II. EXPERIMENTAL

A. Experimental Technique

Measurements have been performed by the backscattering technique using a collimated beam of protons. The apparatus consists of the 2.5-MeV Van de Graaff accelerator of Catania and of a goniometric scattering chamber. The proton beam, collimated within ±0.5 mrad by means of a telescopic arrangement of circular apertures, was kept at an intensity so low (1–10 nA on a 1-mm^2 spot) to produce negligible damage and heating of the target.

The chamber is schematically shown in Fig. 1. As shown, the single-crystal target T is mounted on a metallic-finger pipe F which extends out of the vacuum chamber, thus allowing a thermostatic bath to be introduced. The temperature of the crystal, which is in thermal contact with the bath, can be adjusted over the range 80–500 °K and kept constant within 1 °K. The metallic finger is so mounted that the target remains suspended on the center of a spherical holder H which can be moved from the outside of the chamber by means of a system of micrometric screws S. This arrangement with an optic-lever reading system enabled us to orient the target, within 0.01°, in any space direction. The single-crystal target was usually cut normal to the ⟨111⟩ direction and optically polished. Protons scattered to 150° ∓5° were detected by a conventional surface-barrier detector, with an energy resolution of 7 keV full width at half-maximum (FWHM) at 1-MeV proton energy. The outcoming pulses reached a Laben 4096 multichannel analyzer whose storage capacity was split into 32 groups of 128 channels each; 32 energy spectra could thus be stored, corresponding to different angles between the selected crystallographic direction and the axis of the beam. Figure 2 shows two selected energy spectra corresponding to random and to aligned incidences.

Impurity atoms on the surface, namely, oxygen, carbon, etc., could be detected in the aligned spectrum.[13] They, being lighter than the host, were not observed at the beginning of the measurements because of the low concentration; after a few hours, as soon as their concentration became detectable in the aligned spectrum, the crystal was changed to a new one since the channeling phenomena are quite sensitive to amorphous surface layers.

To reduce these contamination effects as far as possible, the residual pressure inside the chamber

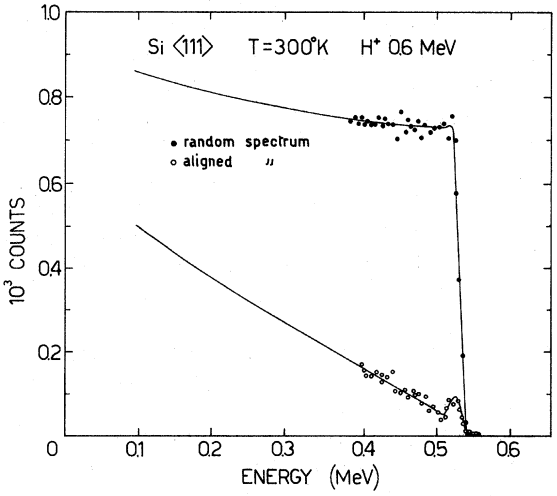

FIG. 2. Energy spectra of 0.6-MeV protons backscattered from Si at room temperature for the beam incident (•) along a random direction and (○) along the ⟨111⟩ axis.

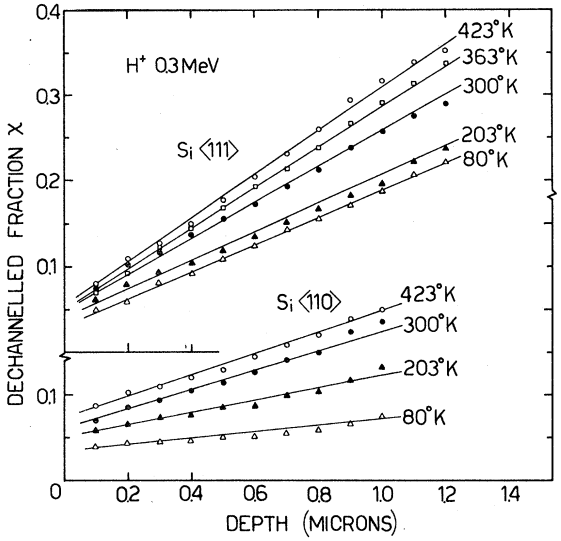

FIG. 3. Depth dependence of the dechanneled fraction χ for 0.3-MeV protons along the ⟨111⟩ and the ⟨110⟩ axes of Si at different temperatures.

was maintained at 10^{-6} Torr and the collision region was surrounded by a liquid-nitrogen trap (see Fig. 1, N). With this arrangement no time dependence of the minimum yield was observed during the measurements, thus showing that the growing contamination layer was thin enough to have no significant effect on the results.

B. Treatment of Experimental Data

The dechanneled fraction $\chi(z)$, as a function of the penetration depth z inside the crystal, has been obtained from the ratio between the aligned and random energy spectra. The energy–to–penetration-depth conversion scales, different for the two spectra, have been obtained by the usual procedure.[5] Moreover, because the energy losses and the ion energies at a given depth are different for the aligned and random spectra, a correction factor has been introduced to account for the energy dependence of the Rutherford cross section. This factor, computed by the energy dependence of the cross section as shown in the random spectrum, is negligible at high energies and low penetration depths, while for 0.3 MeV it amounts to 15% at the maximum considered depth.

Using the same orientation scans, the critical angle $\psi_{1/2}$ has been determined measuring the angular half-width at a level midway between the aligned and random levels. The $\psi_{1/2}$ values at null depth have been obtained extrapolating the $\psi_{1/2}$ values measured at different penetration depths following the previously reported[12,14] procedure.

III. EXPERIMENTAL RESULTS AND DISCUSSION

The aim of this work is, as stated, to study the experimental dependence of the dechanneled fraction χ on the following parameters: the penetration depth z, the target temperature T, and the ion-beam energy E. This fraction has been measured for protons of 0.3, 0.6, and 1.5 MeV impinging on a Si single crystal along the ⟨111⟩ and ⟨110⟩ axes. The crystal temperature has been set at 80, 143, 203, 300, 363, and 423 °K, respectively.

The plots reported in Fig. 3 show the variation of χ vs z for the different target temperatures at 0.3-MeV proton energy. The trend of χ is quite linear with z and it starts from a nonzero minimum value χ_0 at null depth. Both χ_0 and $\chi(z)$ are functions of the temperature, the dependence being stronger for the slopes.

Figures 4 and 5 report similar results for 0.6 and 1.5 MeV energies. The main difference which can be seen among these plots is that the penetration at constant χ increases with increasing energy.

To interpret the above results it should be noted that the dechanneling, which concerns the transition of particles from the aligned to the random beam, requires the explicit considerations of the changes in $E_\perp$. The quantitative treatment of these will be given in detail later on; it can be remarked here, however, that the physical mechanisms which produce the main increase in $E_\perp$ are the fluctuations in the crystalline potential field due to the vibrating nuclei and the collisions of the protons with the electrons. At least the former of these contributions depends on the crystal temperature through

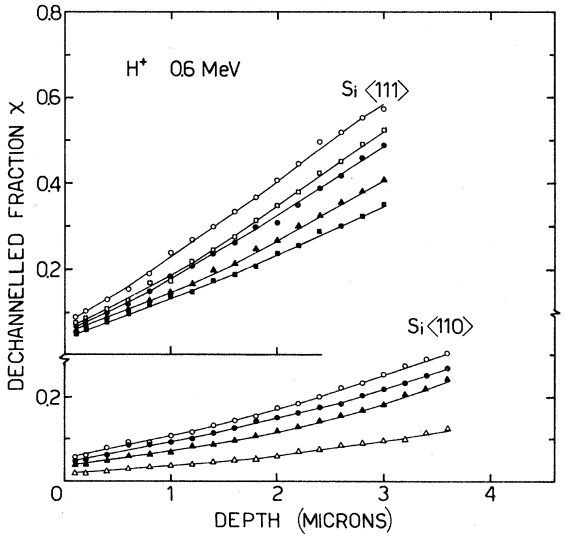

FIG. 4. Depth dependence of the dechanneled fraction χ for 0.6-MeV protons along the ⟨111⟩ and the ⟨110⟩ axes of Si at different temperatures.

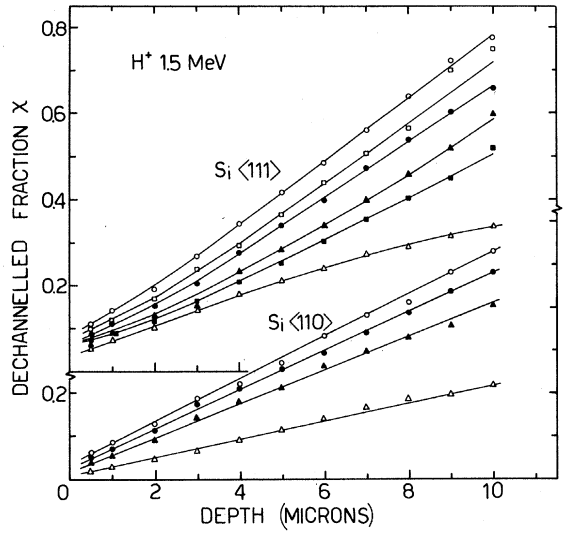

FIG. 5. Depth dependence of the dechanneled fraction χ for 1.5-MeV protons along the ⟨111⟩ and the ⟨110⟩ axes of Si at different temperatures.

the vibrational amplitude. The part of this motion which should be considered, in a first approximation, is that in a plane normal to the ion motion; because of the small angles between the ion path and the atomic string, this part is equal to the amplitude in the plane normal to the atomic string.

This vibrational motion can be described by the Debye mean-square vibrational amplitude normal to the string, i.e., by $\frac{2}{3}$ of the total mean-square amplitude (see, e.g., Ref. 15). If the scattering produced by the vibrating nuclei is the main cause of the changes in the ion transverse energy, the increase in $E_\perp$ and thus the dechanneled fraction should be roughly proportional to the amount of the deviations from the continuous string potential. While the number of deviations is proportional to the penetration depth z, their intensity is proportional to the vibrational amplitude ρ^2. To test the significance of the above description, the $\chi - \chi_0$ values measured at different temperatures have been plotted in Fig. 6 vs the product $z\rho^2$. As can be seen, the curves shown in Figs. 3–5 reduce in this plot to six linear functions, each one characterized by the crystal axis and the ion energy.

Following the same description, one can approach the dependence of $\chi(z)$ on the ion energy. The increase in $E_\perp$ is due to a large number of collisions with the nuclei and the electrons of the crystal, therefore it can be treated by a statistical approach, namely, by multiple scattering. The increase in $E_\perp$, which is related to the angular spreading of the beam, depends roughly on the inverse ratio of the energy[16] both for nuclear and electronic scattering, i.e.,

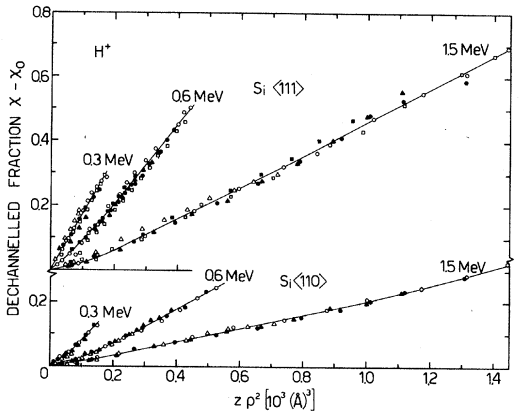

FIG. 6. Dependence of the proton dechanneled fraction $\chi(z) - \chi_0$ on $z\rho^2$ along the ⟨111⟩ and the ⟨110⟩ axes of Si at different temperatures: Δ, 80 °K; ■, 143 °K; ▲, 203 °K; ●, 298 °K; □, 363 °K; ○, 423 °K.

$$\delta E_\perp \propto E(\delta\Omega^2) \propto 1/E ,$$

since

$$\delta\Omega^2 \propto 1/E^2 .$$

The significance of this approach has been verified by plotting the dechanneled fraction $\chi - \chi_0$ vs $z\rho^2/E$; this is reported in Fig. 7. As shown, all the plots of the experimental results, already reported in Figs. 3–6, collapse in two linearlike functions corresponding, respectively, to ⟨111⟩ and ⟨110⟩ channels.

The agreement throughout is quite good, being better at low values of $z\rho^2/E$. The small deviations

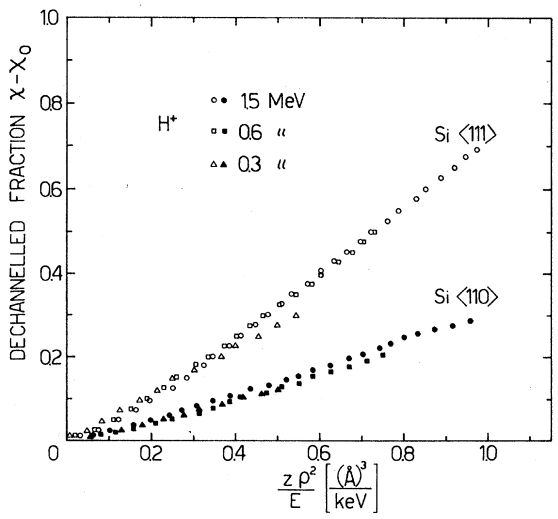

FIG. 7. Dependence of the proton dechanneled fraction $\chi(z) - \chi_0$ on $z\rho^2/E$ along the ⟨111⟩ and ⟨110⟩ axial directions of Si.

appearing at higher values of this parameter can be attributed to the energy losses inside the channel which have been neglected in this plot. These energy losses have, in fact, a dependence on the ion energy which is not of simple inverse proportionality.

The main difference between the ⟨111⟩ and the ⟨110⟩ results is that both the minimum value χ_0 and the slope of the $\chi(z)$ for the ⟨110⟩ direction are about one-half of those for the ⟨111⟩. This result is qualitatively consistent with the lattice geometry; in fact, the transverse area of the ⟨110⟩ channel is larger by a factor of ~2 than that of the ⟨110⟩.

IV. DECHANNELING THEORY

The dechanneling process, as previously said, may be described in terms of particle transitions from the condition of correlated motion inside the channel to the condition of random motion.

The computation of the dechanneled fraction requires (a) knowledge of the initial transverse-energy distribution $E_{\perp 0}$ just beneath the crystal surface, (b) calculation of the changes in $E_\perp$ along the particle path as a function of $E_{\perp 0}$ and of the experimental parameters T and E, (c) definition of a maximum value $E_\perp^+$ above which the particle is dechanneled. This value will be of the order $E_\perp^+ \cong E\,\psi_1^2$, where ψ_1 is the Lindhard critical angle. The actual value will depend on the target temperature. These three aspects will now be discussed.

A. Transverse-Energy Distribution

Consider a collimated beam which enters a single crystal along a close-packed atomic row. The transverse-energy distribution inside the crystal results from (i) the experimental angular spread of the beam; (ii) the angular spreading produced by the amorphous layers covering the crystal surface; (iii) the scattering due to the lattice potential.

The first of these contributions can be described by a Gaussian angular distribution having a width $(\delta\Omega^2)_{expt}$. The second one results from multiple scattering at small angles and from single scattering at large angles.

The Gaussian angular distribution of the beam produced by the multiple nuclear scattering in the amorphous layers and by the experimental spreading is then given by

$$f(\phi)2\pi\phi\, d\phi = (1/\Omega^2)\, 2\phi\, d\phi\, e^{-\phi^2/\Omega^2}\,, \tag{1}$$

where ϕ is the polar angle and $\Omega^2 = (\delta\Omega^2)_{expt} + (\delta\Omega^2)_n$, and where $(\delta\Omega^2)_n$ is the average square fluctuation in angle due to the nuclear multiple scattering and is given by[16]

$$(\delta\Omega^2)_n \simeq (M_2/M_1)\,(\delta E)_n/E\,, \tag{2}$$

$$(\delta E)_n = (4\pi Z_1^2 Z_2^2 e^2 N L_n/M_2 v^2)\delta z\,, \tag{3}$$

where M_1, M_2 and Z_1, Z_2 are the atomic masses and numbers of the projectile and the target atoms, respectively, $(\delta E)_n$ is the energy loss due to the nuclear collisions in a depth length δz, N is the atomic density, v the projectile velocity, and, finally,

$$L_n = (\ln 1.29)[aEM_2/Z_1Z_2\,e^2(M_1+M_2)]\,,$$

a being the Thomas-Fermi (TF) screening radius.

The electronic multiple scattering can be neglected for the amorphous layers since it is much smaller than the nuclear contribution. In terms of transverse energy the distribution probability becomes

$$f(E_{\perp 0})dE_{\perp 0} = (E/\pi E'_{\perp 0})\, e^{-E_{\perp 0}/E'_{\perp 0}}\, dE_{\perp 0}\,, \tag{4}$$

where $E'_{\perp 0} = E\Omega^2$.

The Rutherford single scattering at large angles gives rise to the following distribution in transverse energy:

$$g(E_{\perp 0})\, dE_{\perp 0} = (\hbar^2 E^{1/2}/a^2\,\mu E_{\perp 0}^{3/2})\, dE_{\perp 0}\,, \tag{5}$$

which has been normalized to the total Rutherford cross section for a screened field, μ being the reduced mass. To describe the scattering due to the lattice one may use the continuum string approximation; this approximation could seem too strong a simplification when applied to a few atoms at the beginning of the row. This approximation will be maintained, however, because of its feasibility and for consistency. When a particle enters a crystal, described as a collection of strings, it suffers a deflection. The transverse energy gained in this deflection is $E_{\perp 0} = U(r) - U(r_0)$ and it is equal to the potential at the point of entrance referred to that at the channel axis. If we adopt the above string approximation, only the lattice geometry should be specified.

The computations have been performed for protons entering along the ⟨111⟩ axis of Si. The geometry of this channel (see Fig. 8) is suitable to a simple treatment because the equipotential surfaces can be approximated, for most of the area, with cylinders surrounding a string. Only near the channel axis is there a departure from this symmetry.

The probability that a particle acquires a transverse energy between $E_{\perp 0}$ and $E_{\perp 0} + dE_{\perp 0}$ is equal then to the probability that it enters the crystal at a distance from the string between r and $r + dr$, that is

$$p(E_{\perp 0})\, dE_{\perp 0} = 2\pi r dr/\pi r_0^2\,, \tag{6}$$

where πr_0^2 is the normalization factor equal to the area of the bidimensional unit cell (see Fig. 8).

The relation between r and $E_{\perp 0}$ is given by the standard potential[3]

$$E_{\perp 0} = U(r) - U(r_0)\,,$$

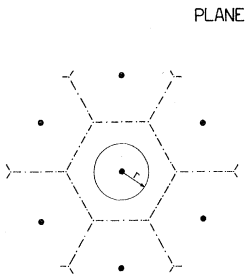

FIG. 8. Si crystal lattice as viewed in the ⟨111⟩ axial direction.

where

$$U(r) = (Z_1 Z_2 e^2/d_{\langle 111\rangle}) \ln(C^2 a^2/r^2 + 1) \tag{7}$$

and

$$U(r_0) = Z_1 Z_2 e^2 (\ln A)/d_{\langle 111\rangle},$$

with $C = \sqrt{3}$, a, the TF screening distance, equal to 0.179 Å, and $A = 1.12$.

The chosen value for A is slightly higher than that derived from the standard potential at the channel axis; it results, instead, in good agreement with the value corresponding to the TF(Moliere) potential. The chosen value seems justified by the rapid drop of the standard potential at large distances.

It should be remarked that the A value affects mainly the initial distribution $P(\epsilon_{\perp 0})$ because the other quantities, namely, $\zeta(\epsilon_{\perp 0})$ (see below) depend mainly on the potential at small distances. The choice made for A does not imply, therefore, any inconsistency throughout, apart from a formal one.

The transverse-energy distribution in terms of $\epsilon_{\perp 0} = 2E_{\perp 0}/E\psi_1^2$ (referred in the following as the "reduced transverse energy"), is then given by

$$p(\epsilon_{\perp 0}) = (C^2 a^2/r_0^2)\,[A e^{\epsilon_{\perp 0}}/(A\, e^{\epsilon_{\perp 0}} - 1)^2]\,. \tag{8}$$

From the reported experimental contributions (4), (5), and (8), we shall now determine the total initial transverse-energy distribution. A simplification can be introduced because $g(E_{\perp 0})$ is negligible with respect to $f(E_{\perp 0})$ for small $E_{\perp 0}$, and vice versa for large $E_{\perp 0}$. We have, therefore, cut and joined these two distributions at the $E_{\perp 0}^*$ value such that $f(E_{\perp 0}^*) = g(E_{\perp 0}^*)$. Finally, the total reduced transverse-energy distribution due to (i)–(iii) is given in terms of $\epsilon_\perp$ by

$$h(\epsilon_{\perp 0}) = \int_0^\infty f(\epsilon'_{\perp 0}) p(\epsilon_{\perp 0} - \epsilon'_{\perp 0})\, d\epsilon'_{\perp 0} \quad \text{for } \epsilon'_{\perp 0} \le \epsilon^*_{\perp 0}\,, \tag{9a}$$

$$h(\epsilon_{\perp 0}) = \int_0^\infty g(\epsilon'_{\perp 0}) p(\epsilon_{\perp 0} - \epsilon'_{\perp 0})\, d\epsilon'_{\perp 0} \quad \text{for } \epsilon'_{\perp 0} > \epsilon^*_{\perp 0}\,. \tag{9b}$$

The integrations have been performed numerically for 0.3-, 0.6-, and 1.5-MeV protons, taking $(\delta\Omega^2)_{\text{expt}} = 0.25\times10^{-6}$ sr, and for an amorphous layer of 1.5×10^{16} -cm^{-2} displaced silicon atoms. (This value has been taken from the area of the surface peak in the aligned spectrum.[13])

From the computed $h(\epsilon_{\perp 0})$ it is then possible to evaluate the integral reduced transverse-energy distribution defined by

$$P(\epsilon_{\perp 0}) = \int_{\epsilon_{\perp 0}}^\infty h(\epsilon'_{\perp 0})\, d\epsilon'_{\perp 0}\,, \tag{10}$$

which gives the fraction of particles having a reduced initial transverse energy larger than $\epsilon_{\perp 0}$; this is plotted in Fig. 9.

B. Changes in Transverse Energy

The changes in the initial transverse energy of a particle along its path inside the channel are due to processes which cause a nonconservation of the transverse energy. The most important process *reducing* the transverse energy is related to the energy loss during the slowing down; the relative decrease is of the same order for both transverse and longitudinal energy. Since the latter is only of the order of 10% at most for the depths considered, one can neglect the corresponding decrease in the transverse energy. The other groups of phenomena responsible for the nonconservation of $E_\perp$ produce an *increase* in the average value of $E_\perp$; they can be summarized as follows: (i) deviations from the picture of the continuum string, mainly due to the atomic thermal motion, (ii) interaction with the electronic density distribution and with its thermal fluctuation, and (iii) defects and impurities present in the crystal.[17]

If the increase in $E_\perp$ vs z is known, one can determine the depth z at which a particle of initial transverse energy $E_{\perp 0}$ reaches the limiting value $E_\perp^+$; it then undergoes the transition from the aligned to the random beam. The contribution of defects can usually be neglected in the crystals adopted for these experiments.

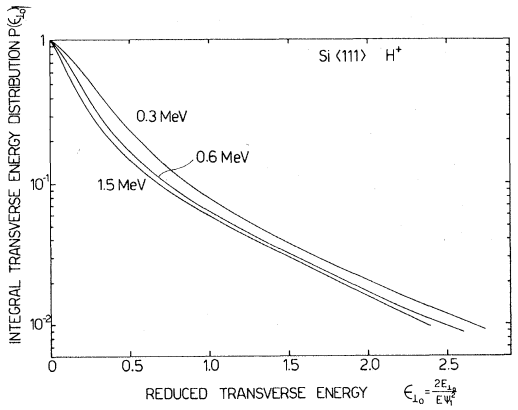

FIG. 9. Integral of the reduced transverse-energy distribution $P(\epsilon_{10})$ vs ϵ_{10} for 0.3-, 0.6-, and 1.5-MeV protons impinging along the ⟨111⟩ axis of Si.

The increase in transverse energy is then due to the angular spreading of the beam produced by multiple nuclear and electronic scattering. In a random system, the increase in Ω^2 (the average square fluctuation in angle) due to nuclear scattering is given by Eq. (2), while that due to electronic collisions is given by

$$(\delta\Omega^2)_e = (m/2M_2E)\, S_e\, \rho(\vec{R})\delta z, \qquad S_e = (4\pi Z_1^2 e^4/mv^2)\ln(2mv^2/I)\,, \tag{11}$$

where m is the electronic mass, $\rho(\vec{R})$ the atomic electron density, S_e is the stopping cross section per electron, and I is the average excitation potential roughly equal to $I_0 Z_2$, with $I_0 = 10$ eV. In the random system, the electronic contribution is always much smaller than the nuclear one, but for a channeled particle which is prevented from close encounters with the nuclei, the two are comparable. The vibrating nuclei contribute to the increase in $E_\perp$ because of the fluctuations $\delta\vec{K}(\vec{r})$ in the transvers force $\vec{K} = -\mathrm{grad}U(\vec{r})$. The changes in $E_\perp$, averaged over the possible transverse positions of the particle, have been reported as[3]

$$\delta\langle E_\perp\rangle_n = (d/4E)\langle \delta\vec{K}(\vec{r})^2\rangle\, \delta z\,. \tag{12}$$

These averages are introduced because a particle with a transverse energy $E_\perp$ undergoes oscillations inside the channel whose amplitude is determined by the minimum allowed distance $r_{\min}$ from the row through the equality $E_\perp = U(r_{\min})$.

The calculations have been carried out for the $\langle 111\rangle$ axis of Si with the same approximation on the shape of the equipotential surfaces made in connection with the evaluation of the transverse-energy distribution. We are then left with a problem of axial symmetry for almost all of the unit-cell area. For axial symmetry, $\delta\vec{K}(\vec{r})$ becomes[3]

$$\langle \delta\vec{K}(\vec{r})\rangle = \tfrac{1}{2}\rho^2\langle K^2(r)/r^2 + K'^2(r)\rangle\,, \qquad K' = \frac{dK}{dr}\,, \quad K = -\frac{dU}{dr} \tag{13}$$

and its average requires the following integration:

$$\langle \delta K(E_\perp)\rangle = [\pi(r_0^2 - r_{\min}^2)]^{-1}\int_{r_{\min}}^{r_0} 2\pi r\, dr\, \delta K(r)\,. \tag{14}$$

From this result and from Eq. (12) one obtains $\delta\langle E_\perp\rangle_n$. The electronic scattering produces a change in the average transverse energy given by

$$\delta\langle E_\perp\rangle_e = (\delta\Omega^2)_e\, E = (m/2M_1)\, S_e\langle\rho(\vec{R})\rangle\, \delta z\,, \tag{15}$$

where the electronic density is related to the potential through Poisson's equation.

To have an idea of the fluctuations in the electronic density due to thermal motion we need a temperature-dependent row potential. If one approximates the atomic vibrations by a Gaussian differential probability

$$f(\rho') = (2\rho'/\rho^2)\, e^{-\rho'^2/\rho^2}\,, \tag{16}$$

the temperature-dependent potential becomes

$$\overline{U}(r) = \int_0^\infty d\rho' \int_0^{2\pi} d\theta\, f(\rho')\, U(\rho'^2 + r^2 - 2r\rho'\cos\theta)^{1/2}\,. \tag{17}$$

Because this integration must be performed numerically, an additional approximation has been made in order to obtain an analytical relation, i.e., the atomic vibrations have been assumed to be isotropic in the plane normal to the string and of constant amplitude ρ. The average potential then becomes

$$\overline{U}(r) = \frac{Z_1 Z_2 e^2}{d} \times \ln\left(\frac{C^2a^2 + r^2 + \rho^2 + [(C^2a^2 + r^2 + \rho^2)^2 - 4r^2\rho^2]^{1/2}}{(r^2 + \rho^2) + |r^2 - \rho^2|}\right). \tag{18}$$

The two potentials (17) and (18) differ significantly only for small distances, while they are about the same for distances $\geq\rho$; the above approximation is then justified.

The increase in the transverse energy $E_\perp$ due to the the reduced electronic scattering has therefore been calculated from (15) and (18). Assuming that the contributions of nuclear and electronic scattering are additive, we obtain for the increase in $E_\perp$ on a path length δz, $\delta\langle E_\perp\rangle = (\delta\Omega^2)_n E\gamma$, where the reduction factor γ is the sum of the nuclear terms γ_n, and of the electronic one which has been divided into a temperature-independent part γ_{se} and into a part γ_{ve} related to the thermal electron-density fluctuations. Thus,

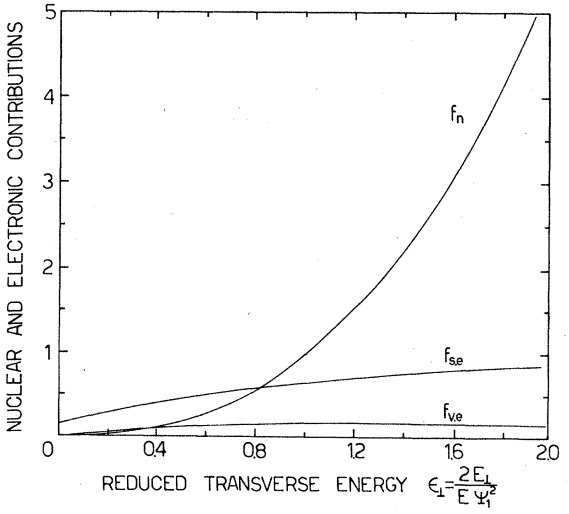

FIG. 10. Plots of the functions f_n, f_{se}, and f_{ve} vs $\epsilon_\perp$ [see text and Eqs. (19) and (20)].

$$\gamma = \gamma_n(E_\perp, \rho) + \gamma_{se}(E_\perp) + \gamma_{ve}(E_\perp, \rho),$$

where

$$\gamma_n(E_\perp, \rho) = \frac{1}{L_n}\,\frac{1}{2}\,\frac{\rho^2}{C^2a^2}\,\frac{Ae^{2E_\perp/E\psi_1^2}-1}{A(e^{2E_\perp/E\psi_1^2}-1)} \times \left[Ae^{2E_\perp/E\psi_1^2}\left(1-\frac{e^{-2E_\perp/E\psi_1^2}}{A}\right)^3 + \frac{2}{3}\left(1-\frac{e^{-2E_\perp/E\psi_1^2}}{A}\right)^3\right], \quad (19a)$$

$$\gamma_{se}(E_\perp) = \frac{1}{L_n}\,\frac{L_e}{2Z_2}\,\frac{Ae^{2E_\perp/E\psi_1^2}-1}{A(e^{2E_\perp/E\psi_1^2}-1)} \times \left(1-\frac{e^{-2E_\perp/E\psi_1^2}}{A}\right), \quad (19b)$$

$$\gamma_{ve}(E_\perp, \rho) = \frac{1}{L_n}\,\frac{L_e}{2Z_2}\,\frac{2\rho^2}{C^2a^2}\,\frac{Ae^{2E_\perp/E\psi_1^2}-1}{A(e^{2E_\perp/E\psi_1^2}-1)} \times \left[\frac{e^{-2E_\perp/E\psi_1^2}}{A}\left(1-\frac{e^{-2E_\perp/E\psi_1^2}}{A}\right)^3\right]. \quad (19c)$$

Finally, in terms of the reduced transverse energy $\epsilon_\perp$, we obtain

$$\delta\epsilon_\perp = [A_n(E,\rho) f_n(\epsilon_\perp) + B_{se}(E) f_{se}(\epsilon_\perp) + C_{ve}(E,\rho) f_{ve}(\epsilon_\perp)]\delta z, \quad (20)$$

separating the quantities which depend on the ion energy and on the target temperature from those which depend on $\epsilon_\perp$.

The functions f_n, f_{se}, and f_{ve} have been plotted in Fig. 10. As shown, the nuclear contribution is the most important for particles having $\epsilon_\perp \gtrsim 1$, while the static electronic contribution predominates for $\epsilon_\perp \lesssim 1$. The thermal fluctuations in the electronic density represent only a small correction throughout and have been neglected in the following.

The same remarks maintain if the factors A_n, B_{se}, and C_{ve} are included, as one can see in Fig. 11 where the functions $F_n = A_n f_n$, $F_{se} = B_{se} f_{se}$, and $F_{ve} = C_{ve} f_{ve}$ are plotted vs $\epsilon_\perp$. Table I shows the computed values A_n, B_{se}, and C_{ve} for several energies of protons and target temperatures. Equation (20) has been integrated to obtain the depth $z(\epsilon_{\perp 0}, \epsilon_\perp^+)$ at which a particle of initial transverse energy $\epsilon_{\perp 0}$ reaches the limiting value $\epsilon_\perp^+$. The integral function $\zeta(\epsilon_\perp)$ is plotted in Fig. 12, as an example, for 1.5-MeV H^+ and for different target temperatures. The difference $\zeta(\epsilon_\perp^+) - \zeta(\epsilon_{\perp 0})$ gives the dechanneling depth $z(\epsilon_{\perp 0}, \epsilon_\perp^+)$.

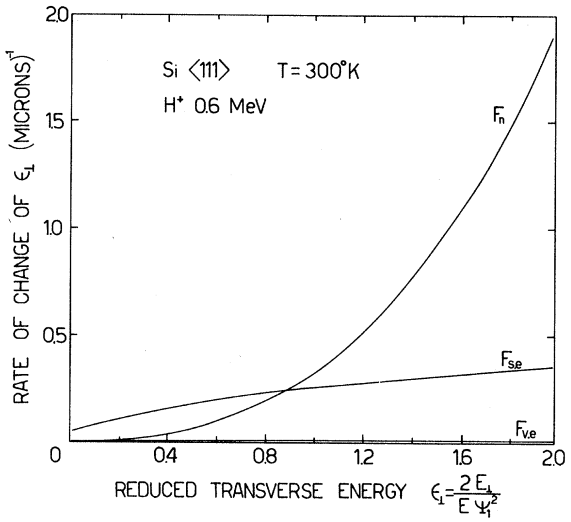

FIG. 11. Plots of the functions F_n, F_{se}, and F_{ve} vs $\epsilon_\perp$ for 0.6-MeV protons on the Si ⟨111⟩ axis at room temperature.

C. Limiting Value $\epsilon_\perp^+$

The maximum allowed value $\epsilon_\perp^+$ for a channeled particle depends on the crystal temperature through $\psi_{1/2}$.[18,19] In fact, $\epsilon_\perp^+ = 2E_\perp^+/E\psi_1^2$ and $E_\perp^+ = E\psi_{1/2}^2$, where $\psi_{1/2}$ is the half-width at half-minimum in the angular scans of the yield, which is a function of the temperature.

TABLE I. Values of the coefficients A_n, B_{se}, and C_{ve} for protons impinging along the ⟨111⟩ axis of Si.

Coefficient (μm^{-1})	Projectile energy (MeV)	Target temperature (°K) 80	143	203	298	363	423
$A_n(E, \rho)$	0.3	0.381	0.504	0.595	0.703	0.751	0.783
	0.6	0.190	0.252	0.297	0.351	0.376	0.392
	1.5	0.076	0.100	0.119	0.140	0.150	0.156
$B_{se}(E)$	0.3	0.547	0.547	0.547	0.547	0.547	0.547
	0.6	0.396	0.396	0.396	0.396	0.396	0.396
	1.5	0.223	0.223	0.223	0.223	0.223	0.223
$C_{ve}(E, \rho)$	0.3	0.084	0.111	0.130	0.154	0.165	0.172
	0.6	0.061	0.080	0.094	0.112	0.120	0.124
	1.5	0.034	0.045	0.053	0.063	0.067	0.070

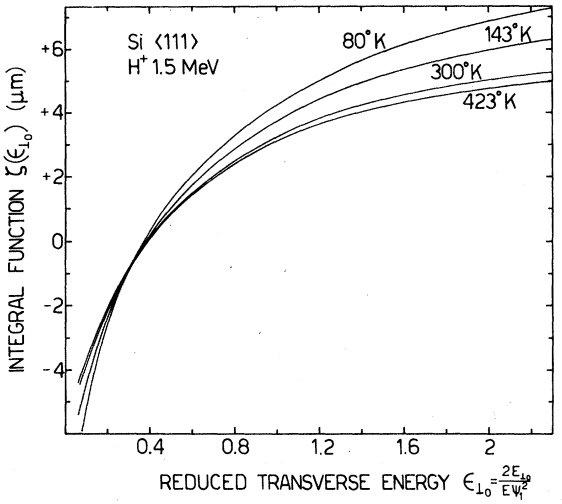

FIG. 12. Integral functions $\zeta(\epsilon_\perp)$ (see text).

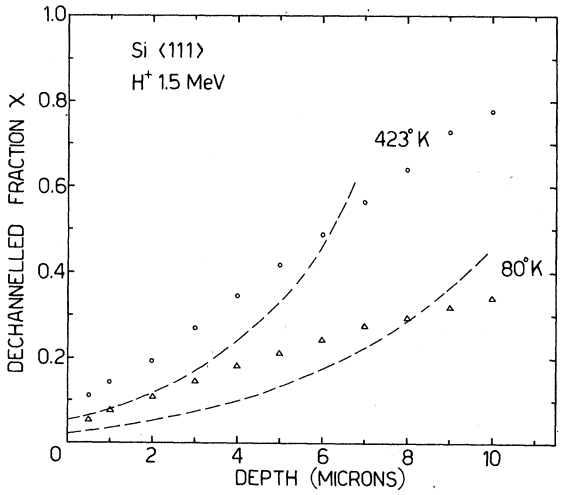

FIG. 14. Experimental and calculated dechanneled fractions for 1.5-MeV protons along the ⟨111⟩ axis of Si at 80 and 423 °K.

The measured $\psi_{1/2}/\psi_1$ values are shown in Table II, and also reported for comparison are the figures calculated by Andersen[20] on the basis of Lindhard's theory. The theoretical values, although showing an over-all agreement with our experimental results, are larger.

V. RESULTS OF CALCULATIONS AND COMPARISON WITH EXPERIMENTS

Knowing the integral of the transverse-energy distribution $P(\epsilon_{\perp 0})$ and the depth z at which the particles escape from the channel, one can plot the dechanneled fraction curves. These computed fractions are shown in Figs. 13 and 14 for 0.3 and 1.5 MeV and for the extreme temperatures. As shown, the calculated plots are in reasonable agreement with the experimental ones, showing the same strong dependence on the target temperature and on the ion energy. The agreement is better at 0.3 MeV for both absolute magnitude and trend, while at 1.5 MeV the calculated plots exhibit a strong upward curvature. The dependence on the experimental parameter $z\rho^2$ is shown in Fig. 15; the agreement is acceptable for low values of $\chi(z) - \chi(0)$, i.e., up to a dechanneled fraction of 25%, while at higher values of χ the calculated values deviate appreciably from the experimental ones; in particular, the computed plots show a temperature dependence stronger than the experimental ones.

It must be remarked that the simple dependence of the experimental dechanneled fractions on the $z\rho^2/E$ parameter does not have a direct correspondence in the theoretical treatment but it results from several contributions, each one having a different and more or less complicated behavior with varying temperature and energy.

In regards to the temperature dependence, since $P(\epsilon_\perp)$ is independent of the temperature, this dependence should be attributed to the reduction factor γ and to the maximum allowed value $\epsilon_\perp^+$. Among

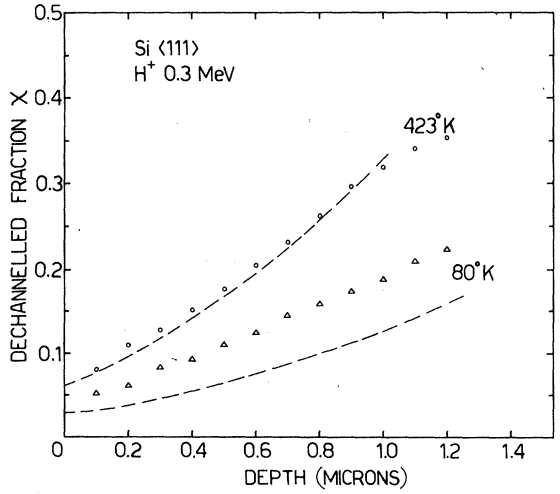

FIG. 13. Experimental and calculated dechanneled fractions for 0.3-MeV protons along the ⟨111⟩ axis of Si at 80 and 423 °K.

TABLE II. Experimental and calculated $\psi_{1/2}/\psi_1$ as a function of the target temperature for protons of energies between 0.3 and 1.5 MeV impinging along the ⟨111⟩ axis of Si.

T(°K)	80	203	298	423
ρ/Ca	0.272	0.313	0.37	0.39
$\psi_{1/2}/\psi_1$ (calc) (Ref. 20)	1.17	1.12	1.05	1.03
$\psi_{1/2}/\psi_1$ (expt)	0.97	0.82	0.79	0.75

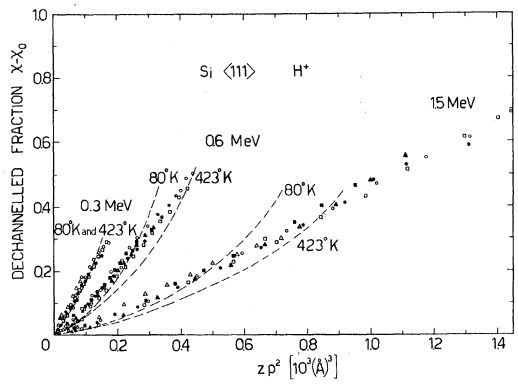

FIG. 15. Experimental and calculated dechanneled fractions $\chi(z) - \chi_0$ vs $z\rho^2$ for 0.3-, 0.6-, and 1.5-MeV protons along the ⟨111⟩ axis of Si.

the different terms of which γ is a sum, there is the temperature-independent electronic scattering which is important at $\epsilon_\perp \lesssim 1$. Since the rate of increase in $\epsilon_\perp$ is much smaller at low transverse energies, particles entering with low $\epsilon_{\perp 0}$ will travel the main part of their trajectories in a region governed by electronic scattering. This fact is partly compensated by the temperature dependence of the critical angle which makes the allowed $\epsilon_\perp^*$ values smaller with increasing temperature.

Regarding the ionic-energy dependence, it should be noted that the factors A_n, B_{se}, and C_{ve} depend inversely on the ion energy, except for a small correction introduced in the electronic terms by the $\ln(E)$. This correction reduces somewhat the energy variation of the γ factors. This factor is compensated, however, by the dependence of the initial transverse-energy distribution on the ion energy. The amorphous layers covering the crystal surface cause a beam angular spreading proportional to $1/E^2$, so that the $P(\epsilon_{\perp 0})$ becomes wider at low energies. The net result is a dependence of $\chi(z)$ on $1/E$.

Some remarks are needed on the upward curvature of the calculated plots. This occurs at high dechanneled fraction, i.e., at large penetration, and thus involves the well-channeled particles having low $\epsilon_{\perp 0}$; it can be attributed to two factors at least. The first concerns the trend of the initial transverse-energy distribution in the region of low row potential, where the mutual interaction of nearest rows is much stronger. The second, perhaps more important, is related to the ion-beam diffusion due to electronic multiple scattering; this diffusion process has been neglected in the present treatment.

VI. CONCLUSION

The results, so far reported, support the hypothesis that the transition of a particle from the aligned to the random beam can be explained in terms of the increase in the transverse energy $E_\perp$.

The significance of the treatment, developed here to describe the dechanneling phenomena, involves several approximations made to handle the problem analytically. Among these the most important are (i) the continuum string approximation for the crystal potential; (ii) the introduction of a parameter A related to the potential at the channel axis; (iii) the description of the thermal motion of the target atoms by an isotropic distribution with constant amplitude; (iv) the neglect of any smearing of the initial distribution by diffusion; for the nuclear term, this approximation is justified by the rapid increase of the reduction factor γ_n with $\epsilon_\perp$ (see Fig. 10), but for the electronic term the diffusion seems to give appreciable contributions; the feeding in has been neglected too, since this would presumably give a term much smaller than the diffusion; (v) the neglect throughout of both the longitudinal- and the transverse-energy losses; this neglect seems, however, quite justified for the relatively small penetrations studied; (vi) use of experimental $\psi_{1/2}$ values to establish the maximum allowed values for the transverse energy of a channeled particle; these values are, however, in semiquantitative agreement with those computed by Andersen[20] using a treatment consistent with the present one.

In spite of these approximations the agreement between the present theory and the experimental results is reasonable. As remarked earlier, the simple dependence of $\chi(z)$ on $z\rho^2/E$ results from several different contributions. Its theoretical meaning is then not straightforward.

One might think that this parameter $z\rho^2/E$ describes, merely by accident, the result in Si; however, it has been shown recently,[21] analyzing the data previously reported by Davies *et al.*,[5] that the same dependence holds true for W. The main difference between the present results and those on W regards the trend of $\chi(z)$ vs z; Davies *et al.* have suggested an exponential decrease with z of the channeled fraction $1 - \chi$. This difference can be justified, however, taking into account the relative magnitude of the nuclear and electronic contributions. In the case of W the electronic contribution is much smaller than for Si so that ions of low $\epsilon_{\perp 0}$ will cross a larger distance in the channel before being dechanneled.[20]

With regard to the planar channeling in Si,[6,22] the trend of the channeled fraction $1 - \chi$ is described quite well, throughout an order of magnitude, by an exponential function of z; the temperature dependence is quite small in this case. The different behavior between the dechanneled fraction for the planar and axial channeling is not surprising. The two cases are described by different kinds of potential, and the transitions from the aligned to the random beam imply the increase in the transverse energy or, respectively, in its component normal

to the plane. The difference may be attributed, therefore, to the different symmetry in the two cases.

Although more detailed investigations, from both the experimental and theoretical points of view, are needed for a full understanding of dechanneling, this process seems useful for studying different scattering mechanisms inside a channel and for deriving information on the crystal potential at large distances from nuclei, i.e., in a region where this knowledge is lacking.

ACKNOWLEDGMENTS

The authors are greatly indebted to Professor J. Lindhard and Professor J. A. Davies for stimulating interest and criticism and to Dr. J. U. Andersen and Dr. E. Bonderup for useful discussions during the course of this work. Thanks are due G. Caruso, S. Pace, G. Panasci, and V. Scuderi for their help in performing the measurements.

[1]S. Datz, C. Erginsoy, G. Leibfried, and H. O. Lutz, Ann. Rev. Nucl. Sci. 17, 129 (1965).

[2]Can. J. Phys. 46, 449–612 (1968).

[3]J. Lindhard, Kgl. Danske Videnskab. Selskab, Mat.-Fys. Medd. 34, No. 14 (1965).

[4]A. Howie, Phil. Mag. 14, 223 (1966); R. E. DeWames, W. F. Hall, and G. W. Lemman, Phys. Rev. 148, 181 (1966); R. E. DeWames, W. H. Hall, and L. T. Chadderton, Phys. Letters 24A, 686 (1967).

[5]J. A. Davies, J. Denhartog and J. L. Whitton, Phys. Rev. 165, 345 (1968).

[6]B. R. Appleton, L. C. Feldman, and W. L. Brown, Brookhaven National Laboratory Report No. 50083, 1967, p. 45 (unpublished).

[7]J. U. Andersen, J. A. Davies, K. O. Nielsen, and S. L. Andersen, Nucl. Instr. Methods 38, 216 (1965).

[8]C. L. Ellegard and N. O. Lassen, Kgl. Danske Videnskab. Selskab, Mat.-Fys. Medd. 35, No. 16 (1967).

[9]L. C. Feldman, B. R. Appleton, and W. L. Brown, Brookhaven National Laboratory Report No. 50083, 1967, p. 58 (unpublished).

[10]K. Morita and N. Itoh, Phys. Letters 31A, 283 (1970).

[11]E. Acerbi, C. Birattari, B. Candoni, M. Castagnoli, G. Dutto, G. Fait, and C. Succi, Nuovo Cimento Letters 3, 569 (1970).

[12]G. Foti, F. Grasso, and E. Rimini, Nuovo Cimento Letters 1, 941 (1969).

[13]J. A. Davies, J. Denhartog, L. Eriksson, and J. W. Mayer, Can. J. Phys. 45, 4073 (1967).

[14]S. T. Picraux, J. A. Davies, L. Eriksson, N. G. E. Johansson, and J. W. Mayer, Phys. Rev. 180, 873 (1969).

[15]R. J. Glauber, Phys. Rev. 98, 1692 (1955).

[16]N. Bohr, Kgl. Danske Videnskab. Selskab, Mat.-Fys. Medd. 18, No. 8 (1948).

[17]For the influence of the defects on channeling see E. Bøgh, Can. J. Phys. 46, 653 (1968).

[18]J. U. Andersen and E. Uggerhøy, Can. J. Phys. 46, 517 (1968).

[19]A. F. Tulinov, V. S. Kulikauskas, and M. Malov, Phys. Letters 18A, 304 (1965).

[20]J. U. Andersen, Kgl. Danske Videnskab. Selskab, Mat.-Fys. Medd. 36, No. 7 (1967).

[21]G. Foti, F. Grasso, R. Quattrocchi, I. F. Quercia, and E. Rimini, Nuovo Cimento Letters 4, 707 (1970).

[22]B. R. Appleton, C. Erginsoy, and W. M. Gibson, Phys. Rev. 161, 330 (1967).